AGU PUBLICATIONS

JGR

Journal of Geophysical Research: Earth Surface

RESEARCH ARTICLE
10.1002/2014JF003328

Key Points:
- Gravel mixtures are immobile downstream of an abrupt GST
- Short suspended sediment advection length scales can make GSTs abrupt
- Interannual variability in flood flows stage sediment through sand bed reaches

Correspondence to:
J. G. Venditti,
jeremy.venditti@sfu.ca

Citation:
Venditti, J. G., N. Domarad, M. Church, and C. D. Rennie (2015), The gravel-sand transition: Sediment dynamics in a diffuse extension, *J. Geophys. Res. Earth Surf.*, *120*, doi:10.1002/2014JF003328.

Received 4 SEP 2014
Accepted 21 APR 2015
Accepted article online 24 APR 2015

The gravel-sand transition: Sediment dynamics in a diffuse extension

Jeremy G. Venditti[1], Natalia Domarad[1,2], Michael Church[3], and Colin D. Rennie[4]

[1]Department of Geography, Simon Fraser University, Burnaby, British Columbia, Canada, [2]Ledcor Technical Services, Vancouver, British Columbia, Canada, [3]Department of Geography, University of British Columbia, Vancouver, British Columbia, Canada, [4]Department of Civil Engineering, University of Ottawa, Ottawa, Ontario, Canada

Abstract As gravel-bedded rivers fine in the downstream direction, they characteristically exhibit an abrupt transition from gravel- to sand-bedded conditions. The prevailing theory for why abrupt gravel-sand transitions emerge is based on bed load sorting of a bimodal sediment. The abruptness is thought to be a consequence of sand overwhelming the gravel-sand mixture once it reaches a critical coverage on the bed. The role suspension plays in the development of gravel-sand transitions has not been fully appreciated. The Fraser River, British Columbia, is an archetypical abrupt gravel-sand transition with a "diffuse extension" composed of a sand bed with some patches of gravel. We examine flow, shear stress, and suspended sediment flux in the diffuse extension to better understand sediment dynamics where the sand bed emerges. Sand is carried in suspension upstream of the primary abrupt gravel-sand transition, but in the diffuse extension, sand is moved as both bed load and suspended load. We do not observe downstream gradients in shear stress or suspended sand flux through the diffuse extension that would suggest a gradual "rain out" of sand moving downstream, which raises the question, how is the sand bed formed? Sediment advection length scales indicate that with the exception of very fine sand that moves as wash load in the diffuse extension, fractions coarser than the median sand size cannot be carried in suspension for more than one channel width. This suggests that sand is deposited en masse at the beginning of the diffuse extension, forming a sediment slug at low flood flows that is smeared downstream at high flood flows to form the sand reach.

1. Introduction

River beds, in the absence of lateral inputs, characteristically fine in the downstream direction [e.g., *Sternberg*, 1875; *Yatsu*, 1955; *Church and Kellerhals*, 1978; *Paola et al.*, 1992; *Rice and Church*, 1998]. Rivers typically have a unimodal gravel-bedded reach, where the bed material fines in the downstream direction, then a bimodal sand-gravel reach, still dominated by the gravel, and finally a unimodal sand-bedded reach as rivers approach base level [*Sambrook Smith and Ferguson*, 1995]. The transition from gravel to sand bed is often observed to be "short" or "abrupt" [*Yatsu*, 1957; *Howard*, 1980; *Shaw and Kellerhals*, 1982; *Paola et al.*, 1992; *Sambrook Smith and Ferguson*, 1995; *Dade and Friend*, 1998; *Knighton*, 1998; *Ferguson*, 2003; *Gran et al.*, 2006; *Gran*, 2012; *Ferguson et al.*, 2011; *Venditti and Church*, 2014], although this is not always the case because the processes of sorting through river bends can extend the transition reach [*Frings*, 2011].

It has been argued that abrupt gravel-sand transitions emerge because fine gravel sizes are unstable and break down to sand size particles [cf. *Yatsu*, 1957; *Kodama*, 1994; *Jerolmack and Brzinski*, 2010], giving rise to a grain size gap somewhere between 1 and 10 mm. While this can happen with certain lithologies, it is not common [*Ferguson et al.*, 1996] and it has been demonstrated that gravel-sand transitions can develop under experimental conditions in which abrasion cannot occur [*Paola et al.*, 1992]. The grain size gap is now thought to be caused by in situ weathering processes at the sediment source [*Wolcott*, 1988] and/or by hydraulic sorting [*Paola et al.*, 1992; *Ferguson et al.*, 1996, 2011]. While abrasion is an important process for downstream fining in river systems, it has little to do with the emergence of an abrupt gravel-sand transition.

More recent work has reasoned that gravel-sand transitions emerge because of grain size sorting processes caused when a river loses the capacity to carry coarser grain sizes [*Brierley and Hickin*, 1985; *Paola et al.*, 1992]. Ferguson and collaborators [*Sambrook Smith and Ferguson*, 1995; *Ferguson et al.*, 1996, 1998, 2003, 2011] have argued that gravel-sand transitions are typically abrupt because of the nonlinear relation between bed shear stress and sediment transport. They argue that as shear stress declines downstream, coarser gravels are

deposited and finer gravel and sand are selectively transported. *Ferguson* [2003], building on an idea of *Wilcock* [1998], used a binary sediment mixture (one size gravel and one size sand) in a numerical model to show that when coarser particles are removed from the upstream sediment supply, a sand bed develops. He suggested that this occurs because sand coverage on the bed surface increases above ~20%. At that point, sand overwhelms the declining gravel fraction, forming a sand bed. However, the binary grain mixture dictates this result, in so far as when the gravel stops moving due to the decline in shear stress, a sand bed must form. *Cui and Parker* [1998] simulated abrupt gravel-sand transitions using gravel with a distribution of sizes, but they did so by changing the way bed load exchanges with the bed material in the gravel and sand reaches, which also forces the transition and its abruptness. Nevertheless, the threshold sand coverage idea is consistent with field [*Ferguson et al.*, 1998] and laboratory experiments [*Paola et al.*, 1992; *Wilcock*, 1998] as well as the idea that a gravel-sand transition occurs when the deposit goes from being framework to matrix supported, posited by some to be a defining characteristic of gravel-sand transitions [*Frings*, 2011; *Venditti and Church*, 2014].

While these insights into the development of abrupt gravel-sand transitions by bed load sorting processes have been useful, the role of sediment suspension has been largely ignored. Deposition from suspension has been acknowledged as a potential mechanism for the development of gravel-sand transitions [*Iseya and Ikeda*, 1987; *Sambrook Smith and Ferguson*, 1996; *Ferguson et al.*, 1998]. However, the idea has not been developed or supported by observations and whether deposition from suspension can form an abrupt transition has not been explored. In recognition of this situation, *Venditti and Church* [2014] examined the downstream change in hydraulics and grain size in the Fraser River, British Columbia, Canada. Their bed material grain size compilation revealed a gravel-sand transition consisting of a terminating gravel wedge with an abrupt shift to sand-bedded conditions (Figure 1d). They further demonstrated that there are patches of gravel downstream of the wedge forming a diffuse extension ~50 km long (72 channel widths).

Venditti and Church [2014] also compiled a 1-D profile of bed and water surface elevation assembled from a bed profile collected in 1999 and segments of the water surface profile in flood measured in the early 1970s and 1999 (Figure 1a). This allowed them to make inferences about how abrupt gravel-sand transitions may emerge via deposition of sand from suspension. The 1-D profile showed a substantial decrease in shear stress at the downstream end of the gravel wedge (Figure 1b) and a consequent abrupt decline in Shields stress leading to the termination of gravel transport (Figure 1c). There was also a substantial decrease in the ratio of shear velocity to settling velocity (Figure 1c), signaling a decline in the ability to maintain a suspended sand load, setting up the sedimentary conditions for a gravel-sand transition.

However, *Venditti and Church* [2014] relied on data from different surveys collected over three decades. They noted that while the broad patterns are robust and repeatable, local variations in shear stress and derivative properties should be viewed cautiously. Furthermore, the morphology of the river is variable through the reaches shown in Figure 1 and a 1-D profile does not accurately represent the local variability in shear stress that leads to sediment transport. We therefore regard the patterns described in *Venditti and Church* [2014] and summarized in Figure 1 as well-informed inferences that require testing. Here we endeavor to test the inference from *Venditti and Church* [2014] that the gravel-sand transition emerges in the Fraser River due to deposition of suspended sand, caused by a change in shear stress at the end of a terminating gravel wedge. Our primary interest lies in how the sand bed forms downstream of the gravel wedge in the diffuse extension. We begin by reviewing previous work on sediment dynamics upstream and downstream of the primary, channel spanning, gravel-sand transition to set the context of our specific research questions.

2. The Gravel-Sand Transition in Fraser River

Fraser River is a spring snowmelt-dominated river with high flows that occur throughout late May, June, and early July, receding in August and September (Figure 2). The basin is large enough (228,000 km^2) that synoptic scale weather events through the rest of the year have only minor influence on the broad river discharge pattern. The mean annual flow into the lower Fraser River is 2830 $m^3 s^{-1}$ at Hope, British Columbia [*McLean et al.*, 1999], the start of the alluvial portion of the river at river kilometer (RK) 165 (measured upstream from the river mouth). The mean annual flood is 8766 $m^3 s^{-1}$, and the 1894 flood, in

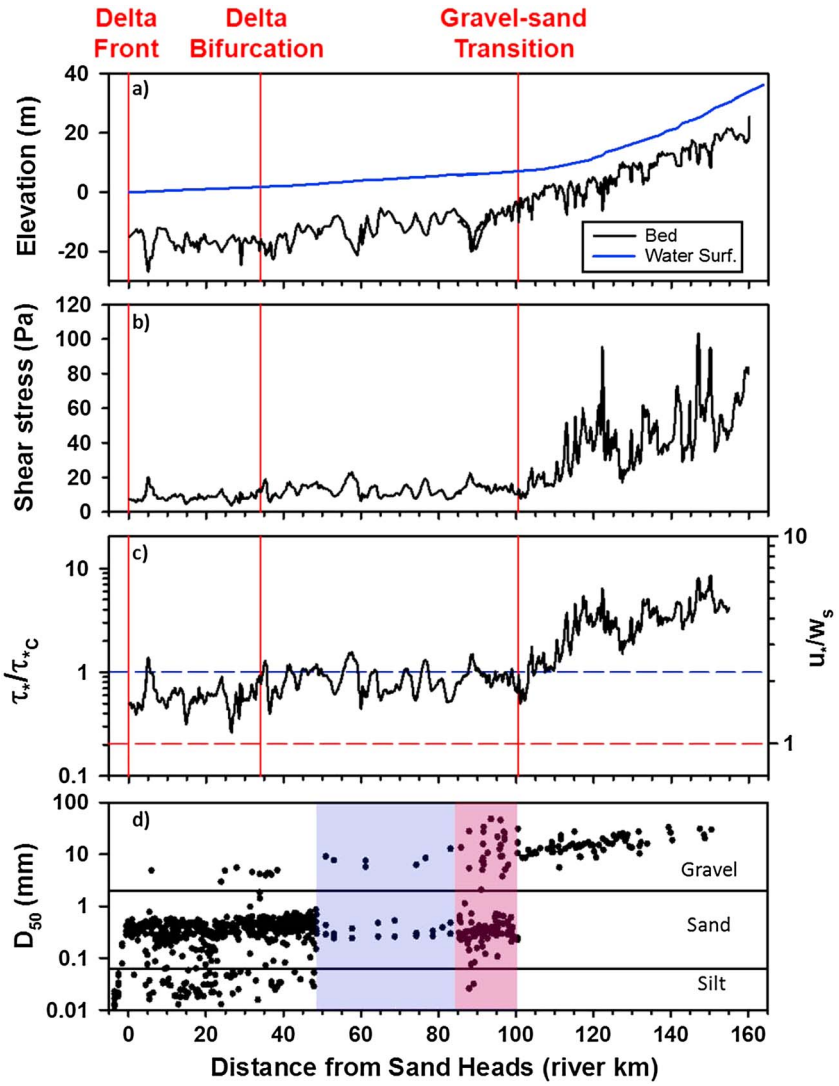

Figure 1. Downstream changes in (a) bed and water surface topography, (b) shear stress, (c) ratio of the Shields stress to the critical Shields stress (τ_*/τ_{*c}) for the median-sized gravel at the transition (10 mm) and a suspension criterion in the form of the shear velocity divided by the settling velocity (u_*/w_s) for the median-sized sand in the sand reach (0.383 mm), and (d) the median grain size. The bed topography is measured in 1999. The water surface profile is from 1999 below RK 85 and 1972 above RK 85. Shear stresses are calculated using these profiles. The red shaded area is our study reach. This and the blue shaded area is the diffuse gravel-sand transition extension. Gravel deposits downstream of the bifurcation are isolated samples that may be of nonfluvial origin. See *Venditti and Church* [2014] for further details.

which flows are estimated to have reached $17{,}000 \pm 1000\ m^3\ s^{-1}$ [*Northwest Hydraulic Consultants*, 2008], is the historic flood of record. The largest gauged flood at Hope was $15{,}200\ m^3\ s^{-1}$ in 1948.

The river is gravel bedded from RK 165 to the tail end of the last major gravel bar complex at RK 100.5, just downstream of a major break in water surface slope that occurs at RK 102 [*Venditti and Church*, 2014]. There is a break in the bed slope at RK 90, suggesting that the gravel-bedded reach of the river forms a terminating gravel wedge with an onlapping sand deposit at the terminus (Figure 1a). Throughout the gravel-bedded reach, the bed material is framework supported (80–90% gravel and 10–20% sand; *McLean et al.* [1999]) and the subsurface median grain size fines downstream from ~30 mm to ~10 mm (Figure 1d). In the channel, sand is a subordinate, interstitially trapped component of the grain size distribution until RK 100.5, where the channel bed becomes almost entirely sand. Some gravel patches persist to RK 48.5: *Venditti and Church* [2014] argued that these patches of gravel form a diffuse extension of the gravel-sand transition. The bed through the diffuse extension is sand, with bimodal sandy gravel deposits in some of

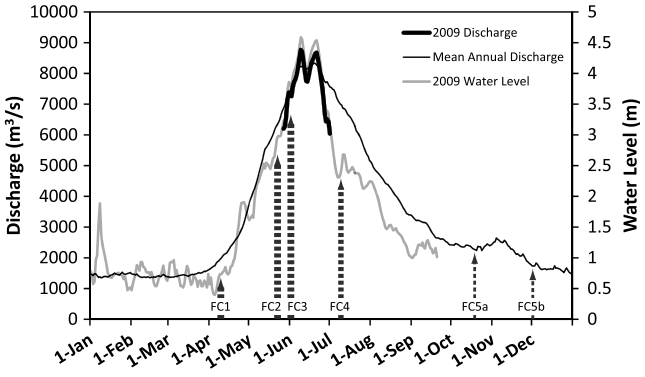

Figure 2. Discharge and water levels for Fraser River at Mission (Water Survey of Canada station 08MH024) for 2009. Also shown are the mean annual hydrograph and the timing of each field campaign (FC1–FC5). The WSC uses a rating curve to calculate discharge (Q) at Mission only when the combined flow at Hope (WSC station 08MF005) and the Harrison River (WSC station 08MG013), a tributary between Hope and Mission, exceeds 5000 $m^3 s^{-1}$ due to the tidal influence on water levels at lower flows, hence, the short duration of the discharge record for 2009. The 59 year mean annual hydrograph is constructed from the sum of the flow from WSC stations 08MF005, 08MG013, and the Chilliwack River at Vedder Crossing (08MH001), another small tributary to the Fraser River near the gravel-sand transition (GST).

the pools, along portions of the thalweg and on the proximal bar surfaces. The bed material sediment supplied from the gravel reach exhibits a grain size gap between 1 and 10 mm [*McLean et al.*, 1999], so while present, these sizes are not abundant.

Sediment dynamics in the gravel reach have been examined quite extensively [*McLean et al.*, 1999; *McLean and Church*, 1999; *Rennie and Church*, 2010]. *McLean et al.* [1999], on the basis of a sediment transport measurement program undertaken between 1966 and 1986 at RK 130.5 (Agassiz, B.C.), showed that sand is carried as wash load in the gravel reach. At this location, sand generally accounts for less than 10% of the channel bed material subsurface, and there is no sand on the surface [*McLean et al.*, 1999, their Figure 10]. Sand sizes up to 1 mm were found in suspension. Sand transport in suspension increases with discharge to the annual flood peak then rapidly declines as it is exhausted from the upstream supply, leaving little sand to be deposited in the channel as the flow recedes. As a result, perennial sand deposits do not exist in the channel. However, transient cover sand deposits on high bar tops and in secondary channels provide source material at higher flows.

McLean et al. [1999] showed that the threshold for significant bed load transport at RK 130.5 is ~5000 $m^3 s^{-1}$, which corresponds to a Shields stress of 0.061, somewhat larger than the typical entrainment threshold for gravel mixtures (0.045) [*Miller et al.*, 1977; *Yalin and Karahan*, 1979), but typical of a structured, armored gravel bed [*Church et al.*, 1998]. Below 5000 $m^3 s^{-1}$, sporadic bed load consisted of a bimodal mixture of sand, with subordinate (<5%) gravel. At ~5000 $m^3 s^{-1}$, the gravel surface layer ($D_{50} = 42$ mm) is entrained and, as flows increase, the bed load increases rapidly and the grain size distribution of the load approaches that of the subsurface bed material ($D_{50} = 25$ mm). Sand makes up a small fraction (about 12%) of the total annual bed load during exceptionally large flood flows. *Rennie and Church* [2010] examined bed movement downstream between RK 116 and 110, where bed surface gravels have $22 \leq D_{50} \leq 35$ mm, using an acoustic Doppler current profiler (ADCP) and found largely the same behavior. They showed that the bed was weakly mobile at ~6000 $m^3 s^{-1}$, corresponding to a Shields stress there of 0.045. These observations, a short distance upstream of the abrupt transition, indicate a bed composed of gravel without extensive sand. The threshold for general movement of the bed material is exceeded annually, which explains the absence of exposed sand in the main channel upstream of the abrupt transition.

There has also been some investigation of sediment dynamics at RK 85 (Mission, B.C.), where the bed material is sand with a subordinate fine gravel mode in some parts of the channel cross section [*McLean*, 1990; *Attard et al.*, 2014]. The D_{10} of composite bed material samples has variously been reported to be 0.177 mm [*McLean et al.*, 1999] and 0.190 mm [*Attard et al.*, 2014]. *McLean et al.* [1999] showed that nearly all the bed load at RK 85 is between 0.177 and 1.0 mm with <0.5% in the gravel range during exceptionally high flood flows. This leads to a nominal division between washload and bed material load of 0.18 mm. Sand makes up ~35% of the average annual suspended load at Mission and roughly half of that is classified as washload.

There have been no observations of sediment dynamics between the main, channel spanning, abrupt gravel-sand transition, where sand presumably is being delivered to the bed, and Mission, 15 km downstream. We are specifically interested in the formation of gravel patches in the diffuse extension and how the sand bed forms. At the outset of our work, we hypothesized that the gravel mixture was immobile in the diffuse

Table 1. Field Campaign Dates, Discharges, and Spatially Averaged Flow Characteristics for Each Field Campaign

Field Campaign	Dates	Mean Daily Discharge ($m^3 s^{-1}$)[a]	$\langle\bar{u}\rangle$	$\langle\tau\rangle$	$\langle u_*\rangle$[c]	$\langle h\rangle$	$0.1 < \langle k_s\rangle < 5$[c]	$\langle u_{*s}\rangle$[c]	$\langle\alpha\rangle = u_{*s}/u_*$[c]
FC1	8–11 April 2009	1058	0.43	1.58	0.036	6.93[a]	0.74	0.0156	0.461
FC2	21–24 May 2009	5680	1.0	9.02	0.091	8.37	0.90	0.0371	0.425
FC3	31 May–3 June 2009	7074 (7368)[b]	1.1	10.1	0.097	8.89	1.13	0.0392	0.412
FC4	9 and 10 July 2009	4857	0.89	7.15	0.080	7.93	0.97	0.0324	0.424
FC5a	18 October 2009	1529	0.54	2.69	0.046	8.12[d]	0.87	0.0198	0.460
FC5b	1 December 2009	2596							

[a]Flows are estimated by summing the preceding day's flow at Hope (Water Survey of Canada station 08MF005), the mean of yesterday and today's flow on Harrison River (08MG013), and today's flow on Chilliwack River at Vedder Crossing (08MH001); the lag periods are estimated by distance from Mission. Estimated flows represent mean discharge delivered to Mission, averaged over the field campaign.
[b]The value in brackets is the discharge reported from the Mission Water Survey of Canada (WSC) station 08MH024 at RK 85. See Figure 2 for an explanation of how flows at Mission are calculated by the WSC. At high flow, tidal effects at Mission create a diurnal variation in the range of 100–200 $m^3 s^{-1}$, hence, the variation between estimated flows and the WSC reported flows.
[c]Values are calculated from spatially resolved values of $\bar{u}$, τ, and h and are then spatially averaged. As a result of nonlinearities in the underlying equations, computation of these variables from spatial averages will produce slightly different values. For example, while $u_* \equiv \sqrt{\tau/\rho}$ at a point, $\langle u_*\rangle \neq \sqrt{\langle\tau\rangle/\rho}$.
[d]This value is influenced by the tidal effects on the river at low flows.

extension based on the work by *Venditti and Church* [2014] (Figure 1c) but could leak out of the gravel wedge because of the effect of sand on gravel mobility. In order to assess this hypothesis, we require shear stress measurements in the diffuse extension reach.

We also hypothesized at the outset of our work that sand gradually rained out of suspension downstream of the gravel wedge, thickening the sand bed. This would require a downstream decline in shear stress and suspended sediment flux. However, to first approximation, shear stress appears to increase through the initial portion of the diffuse extension (RK 100–85; Figure 1b), which seems an unlikely scenario to develop a sand bed because increasing shear stress would cause erosion, not deposition. It is more probable that this local pattern results from inadequate representation of shear stress by the 1-D profile through this reach, where slope is constant and flow depth is increasing. In order to test the hypothesis that sand is raining out of suspension in this reach of the river to form the sand bed, we require measurements of shear stress and suspended sediment flux as directly as possible in the diffuse extension.

In this paper, we present shear stress and suspended sediment flux measurements as well as computed potentials for gravel mobility as bed load and sand mobility in suspension in the initial reach of the diffuse extension. We do not know where in the channel to measure these properties to get suitable averages, so we take spatially resolved measurements. Furthermore, we do not know the role that annual variability in flow plays in gravel mobility and sand deposition, so we measure shear stress and suspended sediment flux at different flows. We use these data to explore the advection lengths of suspended sediments in the reach immediately downstream of the terminating gravel wedge in the Fraser River. We directly address the following questions: (1) How does gravel mobility influence the morphology of the gravel-sand transition?; (2) What is the spatial and temporal pattern of sand deposition to the bed?; (3) Can an abrupt gravel-sand transition emerge due to a change in sediment suspension?

3. Methods

3.1. Observations

Bed topography, flow, and suspended sediment concentrations were mapped using a Teledyne RD Instruments 600 kHz Workhorse Rio Grande acoustic Doppler current profiler (ADCP) mounted on a 5.5 m aluminum boat. The ADCP was connected to a Trimble GPS Rover operating in real time kinematic mode which gave vertical and horizontal positions accurate to tens of millimeters. Mapping was done between RK 85 and RK 100.5 in five campaigns over the 2009 freshet, corresponding to (1) prefreshet low flow (FC1), (2) rising limb of the hydrograph (FC2), (3) near-peak flow (FC3), (4) declining limb of the hydrograph (FC4), and (5) postfreshet low flow (FC5) (Table 1). Figure 2 shows the field campaigns in relation to flow and water level at Mission. Flow peaked at ~9000 $m^3 s^{-1}$ at Mission, which is just below the mean annual flow of 9790 $m^3 s^{-1}$ [*McLean et al.*, 1999]. During each field campaign, the boat moved upstream while traversing the river in a "zigzag" pattern (Figure 3a). The zigzag pattern is optimal for this

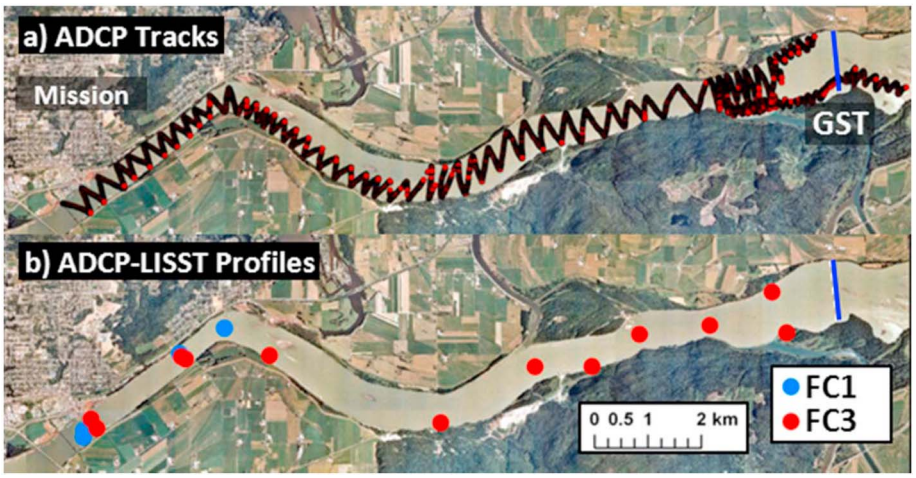

Figure 3. (a) The zigzag pattern used for ADCP data collection field campaign 1 (FC1) and (b) the locations of LISST profiles used to develop the ADCP backscatter—suspended sediment concentration correlation.

type of data collection as it ensures most assured boat control, maximum survey continuity, greater spatial coverage, and reduces interpolation errors [*Rennie and Church*, 2010].

In order to use the ADCP to measure suspended sediment concentrations, we also deployed a Sequoia Laser In Situ Scattering and Transmissometry 100X (LISST-100X) that measured suspended sediment concentrations and particle size distributions in 32 logarithmically spaced size classes between 2.5 and 500 μm. The LISST-100X was enclosed in a metal cage and drag-reducing housing and was deployed from a stern-mounted davit on an 11 m fishing vessel. Attempts were made to collect LISST data during all ADCP campaigns except campaign 4. However, successful deployments were made only during field campaigns 1 (low flow) and 3 (near-peak flow). The boat was anchored at locations in the reach to collect vertical LISST profiles at various depths. Each at-a-point sample was 5 min long and sampled at 1 Hz (300 samples per point in a profile). The LISST measurements were obtained exclusively to calibrate the ADCP, which requires variability in concentration. Our choice of various locations for profiles and measurements at different heights above the bed provided the necessary variability. In order to obtain coincident ADCP measurements during LISST profiles, the smaller aluminum ADCP boat was tethered to the larger anchored vessel. The separation between the instruments was ~2 m. The 5 min integration time ensures that the mean concentration and backscatter were representative of the sediment concentration at each instrument position. During the two successful LISST field deployments, a total of 17 simultaneous LISST and ADCP profiles were collected.

3.2. Data Analysis

A software package developed by Rennie and collaborators [e.g., *Rennie and Millar*, 2004; *Rennie and Church*, 2010] was used to extract the ADCP data and correct for the magnetic variation, depth of the transducer below the surface, and height of the GPS receiver above the instrument. Following the approach described by *Rennie and Church* [2010], shear stress was estimated by calculating shear velocity (u_*) from the law of the wall

$$\frac{u}{u_*} = \frac{1}{\kappa}\ln\left(\frac{z}{z_o}\right) \tag{1}$$

where u is the velocity at height z above the mean bed elevation, κ is the von Kármán constant (0.41), and z_o is the plane of zero velocity above the bed. The shear velocity was calculated as $u_* = \kappa m$, where m is the slope of a regression through $\ln(z)$ and u. We back calculated z_o from measured velocity at a specific height above the bed and calculated the roughness height in the channel as

$$k_s = 30 z_o. \tag{2}$$

A moving average of 11 adjacent ADCP profiles was used when calculating u_* because single ping velocity profiles are relatively noisy [*Rennie and Church*, 2010]. Theoretically, the law of the wall is strictly applicable to the lower 20% of the velocity profile in steady, uniform flow. However, the lower 6% of data are removed

from ADCP profiles due to sidelobe effects, and there are often only 1–2 data points between 6 and 20% of the depth in our data set, which makes it difficult to satisfy this criterion. We therefore elected to use the whole velocity profile in our analysis as recommended by *Rennie and Church* [2010]. *Sime et al.* [2007], using measurements from the same river, showed that a calculation based on mean velocity and the zero-velocity elevation gives more precise results but requires an a priori estimate of k_s, the roughness height, which is not available for our areally extensive surveys with seasonally changing bed conditions. To ensure that the velocity profile was satisfactorily semilog linear, shear velocity estimates were filtered out if calculated k_s exceeded 5 m or was less than 0.1 mm [*Rennie and Church*, 2010]. Shear stress (τ) was calculated from shear velocity as

$$\tau = \rho u_*^2 \tag{3}$$

where ρ is the density of water.

We selected natural neighbor interpolation to generate spatial maps of flow parameters over the more commonly used kriging method, which proved to be a poor method to represent spatial patterns in our data set [*Domarad*, 2011]. Kriging is a nonlocal interpolation method based on regionalized variable theory that assumes that the spatial variation in a variable is statistically homogeneous throughout the surface. In our data set, the separation between locations along the left or right bank, where we turned the boat, could be relatively large (order 100 m), compared with similar data gathering exercises where kriging was successfully used [e.g., *Rennie and Church*, 2010]. As such, the spatial variation in a variable was not homogeneous and produced obvious interpolation errors. Natural neighbor interpolation is a local method that uses only a subset of samples that surround a query point. It finds the closest subset of input samples to a query point and applies weights to them based on proportionate areas in order to interpolate a value [*Sibson*, 1981]. Natural neighbor interpolation produces a surface that passes through the input samples and is smooth everywhere except at locations of the input samples. It adapts locally to the structure of the input data and requires no input from the user pertaining to search radius, sample count, or shape. It works equally well with regularly and irregularly distributed data [*Watson*, 1992]. We interpolated the data using a variety of different grid densities but decided to use an 80 m density, which is larger than the mean separation of the lines composing the zigzag pattern.

Review of the LISST data revealed irregular spikes in the largest two grain size classes and an increase in the smallest four grain sizes, which is physically unreasonable. This commonly occurs because these grain size bins are at the edge of the laser detector admittance. If the laser alignment is not perfect, these bins are susceptible to large errors (Sequoia Scientific, personal communication, 2009). These grain size classes were removed from the distributions, making the effective range of the LISST observations 4.85 to 359 μm which should index the suspended sediment concentration well in the study reach.

3.3. Correlation of LISST SSC and ADCP Backscatter

RD Instruments ADCPs record the reverberation level (backscatter) as echo intensity recorded in counts, which can be used to estimate suspended sediment concentration (SSC) in rivers [e.g., *Gartner*, 2004; *Wall et al.*, 2006; *Bradley et al.*, 2013]. Backscatter strength is a function of sediment particle size, type, and concentration; thus, backscatter is directly proportional to concentration for a constant sediment type and size [*Thorne and Hanes*, 2002]. Echo intensity is converted to measured backscatter as

$$RL = sf \times EI. \tag{4}$$

wherein *sf* is an instrument specific scale factor obtained from RD instruments. The forward facing beam was selected for this analysis, which has *sf* = 0.3979 dB/count. The measured backscatter is corrected for two-way transmission losses caused by beam spreading and fluid attenuation by applying the logarithmic version of the sonar equation to calculate the fluid-corrected backscatter (FCB) from

$$\mathrm{FCB} = \mathrm{RL} + 20\log_{10}(r) + 2\alpha_f \tag{5}$$

where r is the distance along the acoustic beam. The water absorption coefficient α_f is computed for zero salinity [*Schulkin and Marsh*, 1962] from

$$\alpha_f = 8.686 * 3.38x10^{-6}\frac{f^2}{f_T} \tag{6}$$

$$f_T = 21.9x10^{\left(6-\frac{1520}{T+273}\right)} \tag{7}$$

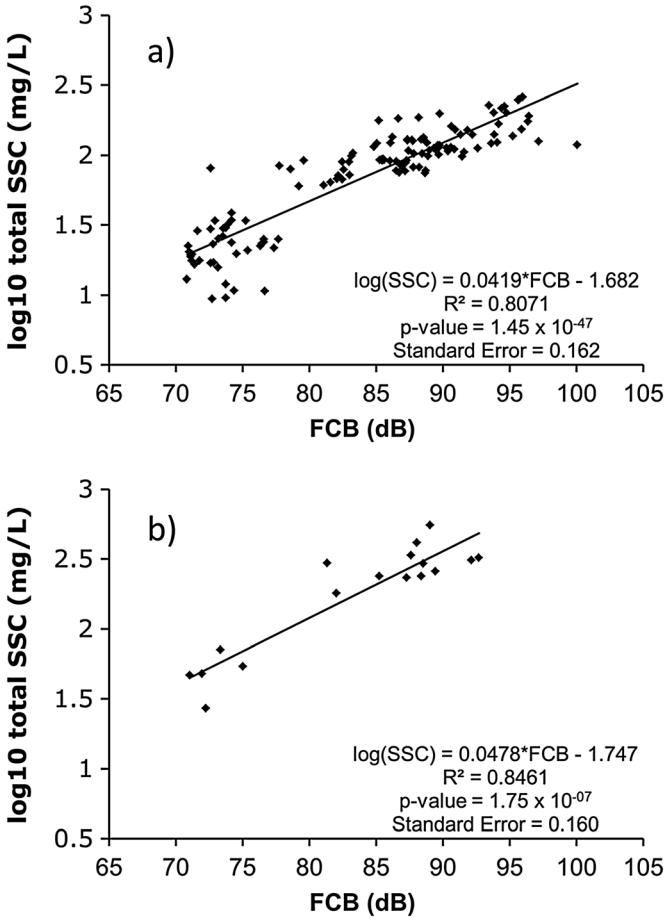

Figure 4. Correlation between SSC and FCB for (a) collocated LISST 100 samples and the FCB in the nearest ADCP elevation and (b) depth-averaged LISST 100 and ADCP FCB profiles.

where f is the frequency of the ADCP and T is the water temperature in degrees Celsius. Sediment attenuation should theoretically be negligible for the combination of transducer frequency, sediment size, sediment concentration, and distance from the transducer used in our measurements [*Flammer*, 1962; *Urick*, 1948] so we ignore it. In order to calculate the suspended sediment concentration (SSC) from FCB, we use the following relation, due to *Gartner* [2004]:

$$\mathrm{SSC} = 10^{(a * \mathrm{FCB} + b)} \tag{8}$$

wherein a and b are the slope and intercept of a least squares regression between the LISST-derived SSC and FCB (Figure 4). We correlated the collocated measurements at specific heights above the bed (Figure 4a) as well as depth-averaged LISST SSC against depth-averaged FCB (Figure 4b). We elected to use the latter correlation in our further analysis because the vertical gradients in SSC and grain size violate the assumption of constant grain size and concentration in the derivation of the sonar equation. Nevertheless, the difference between the collocated and depth-averaged correlations is not so great as to affect our results or interpretations [*Domarad*, 2011]. The 95% confidence intervals for the correlation slopes overlap, meaning the two equations are the same within statistical precision.

4. Results

4.1. Patterns of Velocity and Shear Stress

Figure 5 shows the spatial patterns of depth-averaged velocity $\bar{u}$ through the initial 15 km downstream of the gravel wedge for each field campaign (see Table 1 for dates and discharges). At the upstream end of the reach is Yaalstrick Bar, the last major gravel bar complex in the system, which terminates at RK 100.5. The channel is straight with a sinuous thalweg to Hatzic Bar, which is a concave-bank bench composed primarily of sand with a gravel veneer at its head [*Venditti and Church*, 2014]. Hatzic bend maintains one of the most deeply scoured holes in the river (~35 m at high flow). The Mission Reach extends downstream to RK 85 and is sand bedded with patches of gravel along the north bank [*Venditti and Church*, 2014]. Velocity increased from FC1 to FC3, then declined from FC3 to FC5. High $\bar{u}$ follows along the sinuous thalweg between RK 100.5 and Hatzic Bar at all flows. At peak flow (FC3), the high $\bar{u}$ through the Mission Reach (from Hatzic Bend to Mission) occurs along the north bank, scouring the bed of sand, while at lower flows, that pattern does not appear. At Yaalstrick Bar, at the upstream end of the reach, there is an interesting shift in the velocity pattern between high flow (FC2 and FC3) and the declining limb of the hydrograph (FC4). At the higher flows, there is a persistent high velocity zone in the shallow water over the tail end of Yaalstrick Bar. On the receding limb of the hydrograph, this same area is a low-velocity zone, which likely leads to sand deposition on the bar. A low-velocity zone persists over Hatzic Bar at all flows, which shows why it is a depositional element in

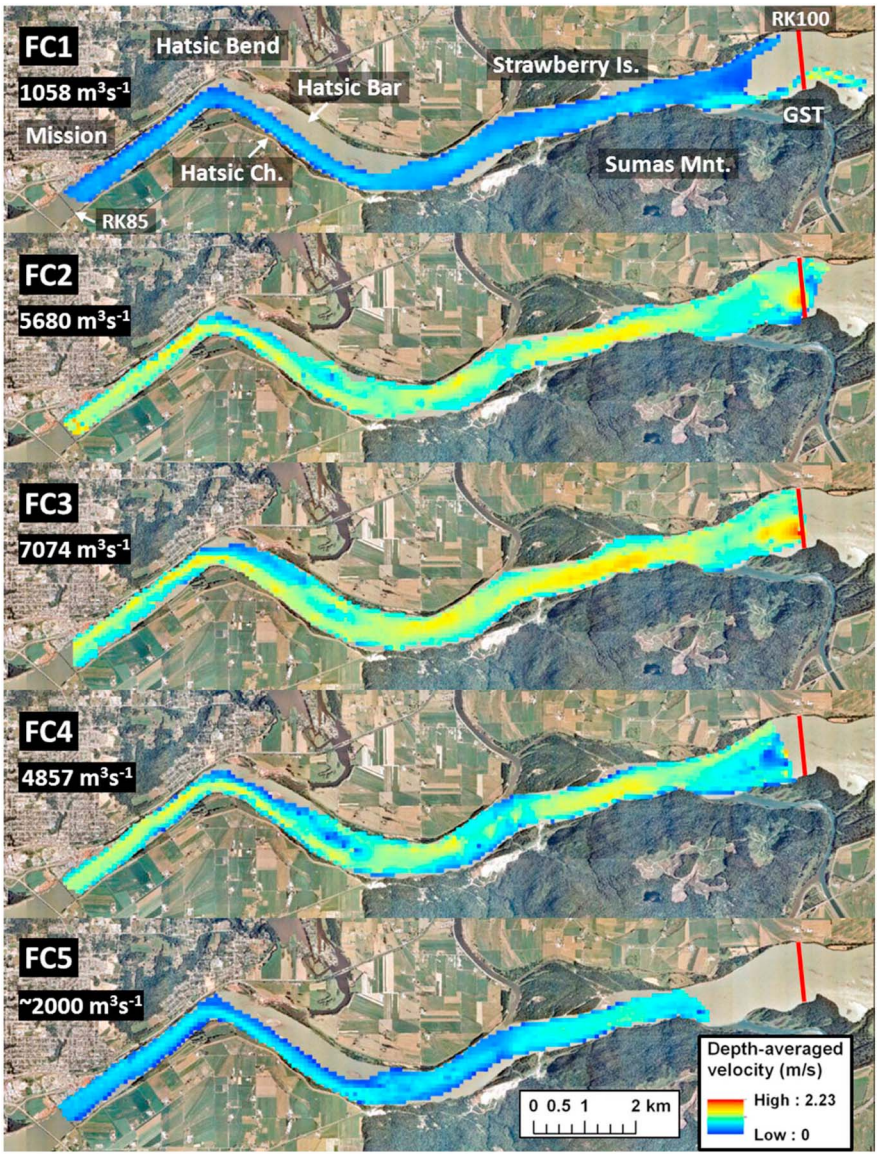

Figure 5. Depth-averaged velocity for all field campaigns interpolated at 80 m resolution. The red line marked GST is the end of the gravel wedge identified as the gravel-sand transition by *Venditti and Church* [2014].

the channel and explains the downstream fining sequence observed there by *Venditti and Church* [2014]. Significantly, beyond the end of Yaalstrick Bar, we detect no overall downstream trend of velocity in the reach.

Patterns similar to those of $\bar{u}$ are observed in shear stress τ (Figure 6). Stresses increase from FC1 (low flow) to FC3 (peak flow), then decline to FC5. At high flow, τ is higher over the tail end of Yaalstrick Bar, along the sinuous thalweg, and along the north side of the Mission Reach. Again, there is no obvious downstream change in shear stresses through the studied reach that would indicate that sediment transport should decrease, but there are curiously high shear stresses along the margin of the channel just off Strawberry Island at low flow (FC1 and FC5). A submerged extension of the channel around Strawberry Island affected velocity profiles at this location. There were also elevated shear stresses at high flow (FC2 and FC3) in Hatzic Channel on the left bank downstream of a channel bend. These high shear stresses were likely due to secondary circulation patterns induced by the channel bend [*Dietrich and Whiting*, 1989; *Kashyap et al.*, 2012]. It is noteworthy that recent bank failures were observed at this location.

The total boundary shear stress in the reach can be estimated as

$$\tau_T = \rho g S h \tag{9}$$

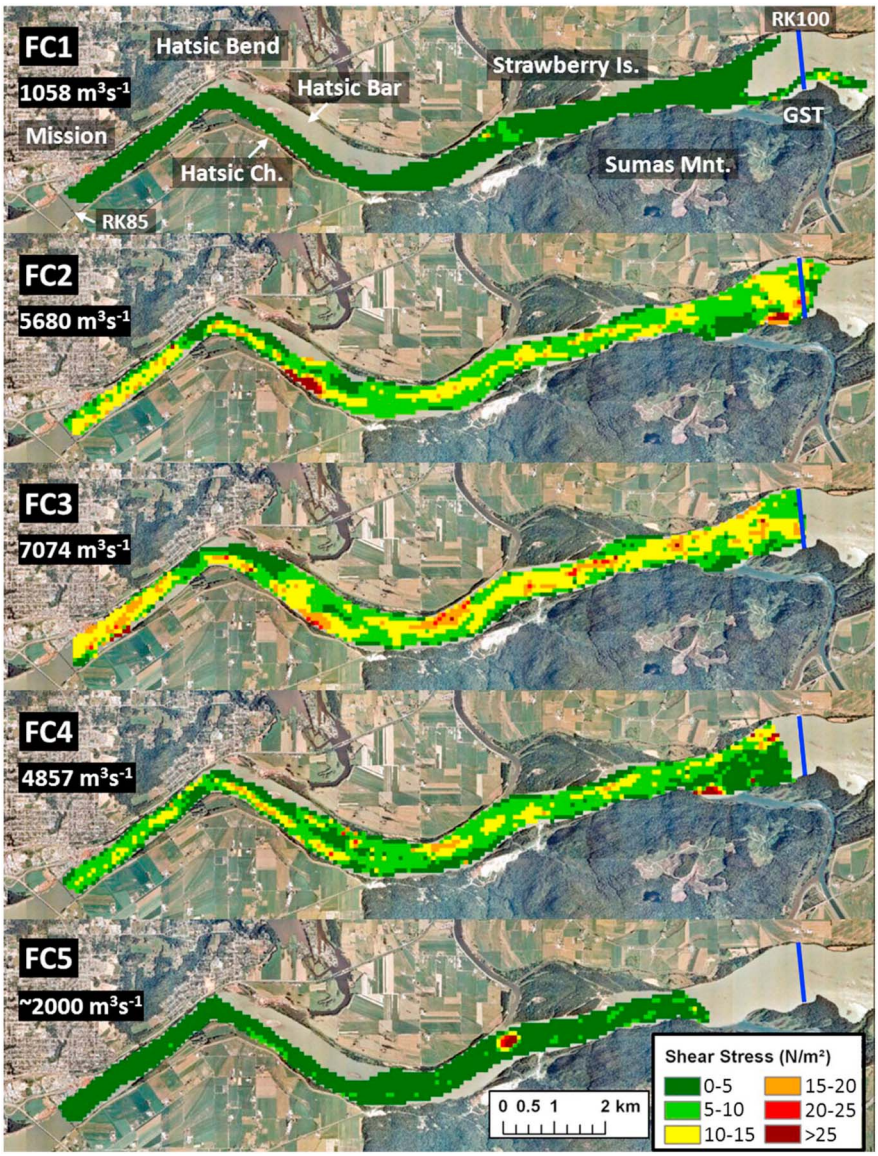

Figure 6. Total shear stress for all field campaigns interpolated at 80 m resolution.

where g is the gravitational acceleration, S is the water surface slope, and h is the flow depth. Using historical records of water surface and bed elevation from 1972, 1974, and 1999, *Venditti and Church* [2014] found that τ_T varied from 5 to 25 Pa, with a mean value of ~13 Pa in the study reach. In Figure 6, the range in τ is similar (0.23–27 Pa), but the mean is lower (10 Pa) because the coverage includes the channel edges. Furthermore, the flows in 1972, 1974, and 1999 were some of the highest on record with recurrence intervals of 50, 13, and 14 years, respectively. The lesser mean shear stress for the 2009 flow, with a recurrence interval of 2 years, is not surprising. Importantly, the similarities between the ranges of measured shear stress suggest that the 2009 flow should represent the patterns in shear stress quite well. It is also revealing that stresses computed for the high floods are not dramatically different than those observed in 2009.

4.2. Size-Specific Shields Stress for Gravel

We examined the potential for gravel mobility in the reach using the nondimensional Shields stress calculated as

$$\tau_* = \frac{\alpha\tau}{(\rho_s - \rho)gD} \tag{10}$$

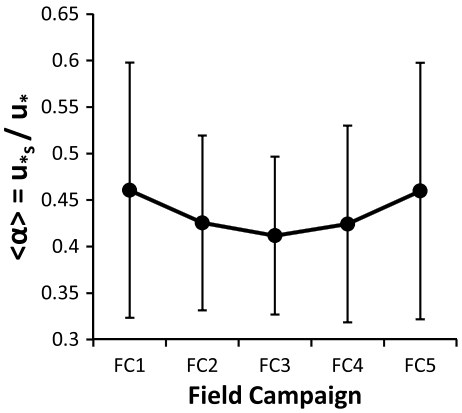

Figure 7. Ratio of grain-related shear velocity to the total shear velocity (α) for each field campaign. The error bars are ±1 standard deviation about the mean.

where τ is from Figure 6, ρ_s is the sediment density, D is a grain size, and α is the fraction of the total shear stress applied to the bed and capable of moving sediment. We refer to this as the potential mobility of various grain sizes, because we do not have direct observations of how different particle sizes are moving in the reach. So this calculation tells us whether or not different size classes would be mobile if present at the location. We estimated α by calculating the shear velocity associated with the sand roughness in the reach using the depth-averaged version of the law of the wall:

$$\frac{\overline{u}}{u_{*_s}} = \frac{1}{\kappa}\ln\left(11\frac{h}{k_{ss}}\right) \tag{11}$$

where u_{*s} is the value of u_* that would occur in the absence of form roughness in the channel, and $k_{ss} = 2D_{50}$ of the sand [*van Rijn*, 1993]. We elected to use the sand D_{50} because the channel is dominated by sand throughout the thalweg in the study reach (Figure 1). We calculate the effective shear stress coefficient as

$$\alpha = u_{*_s}/u_*. \tag{12}$$

The mean value of total roughness k_s in the reach, calculated from equations (1) and (2), increased with the discharge from 0.74 m at low flow (FC1) rising to 1.13 m at high flow (FC3) then declining back down to 0.84 m following the freshet (FC5). This pattern in k_s reflects the development of sand dunes in the reach. The mean values of α also varied with discharge in the channel, decreasing at high flow as bedforms became larger, but the values were all within ±1 standard deviation of one another (Figure 7). So we elected to use the mean value of $\alpha = 0.46$ for all the field campaigns in our application of equation (10).

Figure 8 shows the size-specific Shields stress of gravel through the reach for the low flow (FC1; Figure 8a) and the high flow (FC3; Figure 8b) conditions. We can estimate the potential for a particle to be mobile, if present at the location, by comparing the value of τ_* to its critical value for entrainment τ_{*c}. Because of "hiding" and "exposure" effects in particle mixtures, gravel beds tend to have a constant entrainment threshold of $\tau_{*c} \approx 0.045$ [*Miller et al.*, 1977; *Yalin and Karahan*, 1979]. Our approach explicitly ignores the effect of sand on gravel mobility. If the applied shear stress is near the threshold required for gravel entrainment, the presence of sand can reduce τ_{*c} by as much as 2 times in the empirical model of *Wilcock and Crowe* [2003]. At coverages less than 30%, the effect is lesser. At coverages greater than 30%, the bed is dominated by sand. Unfortunately, we cannot measure the sand coverage on gravel patches in the diffuse extension reach because mean flow depth is 7–9 m. Fortunately, the reach is mainly sand bedded, so the 30% threshold has been exceeded and we are really exploring what grain sizes would be theoretically mobile if they were present on the bed.

Figure 8 shows some spatial variability in τ_* which is consistent with the increases and decreases in shear stress along the sinuous thalweg through the reach. Figure 8a (see 2 mm size class) shows that at low flow, there is a weak downstream gradient in τ_*, which reflects a weak downstream gradient in shear stress that also occurs during FC5, but at no other flows. At low flow, 2 mm particles are potentially mobile in areas of anomalously high shear stresses, but are otherwise immobile, as are larger grains. At high flow (Figure 8b), there are no apparent downstream gradients in τ_*. There are a few patches on the bed where τ_* for 8 mm grains exceeds the nominal threshold of $\tau_{*c} \approx 0.045$ and more extensive areas where τ_* exceeds 0.03. These areas could have mobile gravel in the presence of sand coverage $<30\%$, but the areas of high shear stress do not correspond to patches of gravel in the reach. Grains greater than 8 mm are immobile throughout the reach.

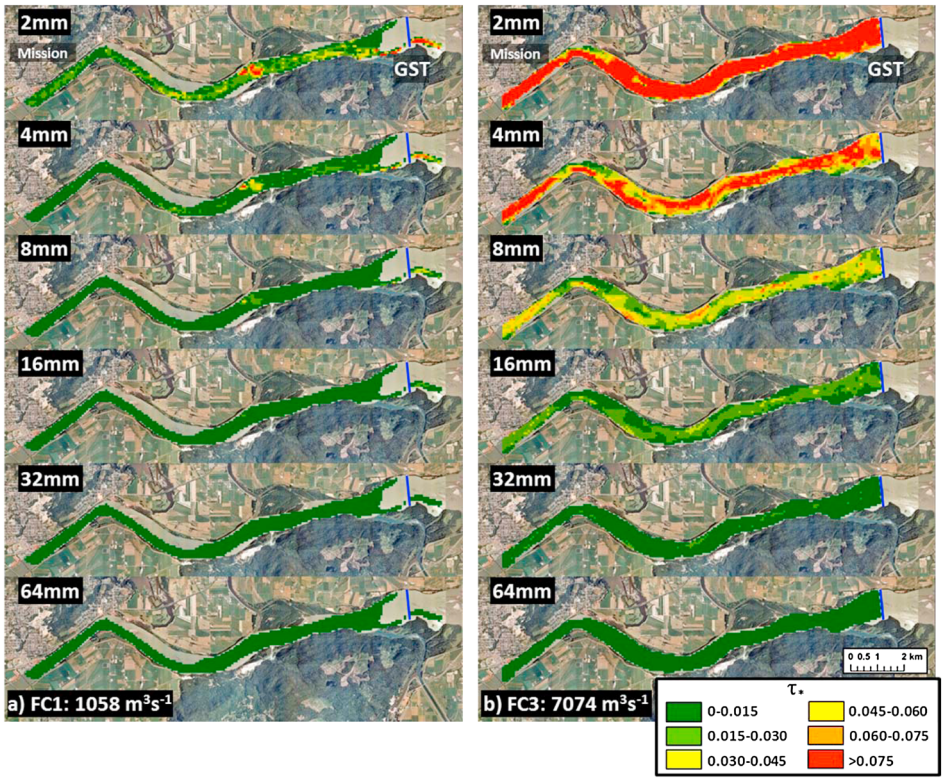

Figure 8. Shields stress for gravel-sized material at (a) low flow (FC1) and (b) high flow (FC3). Where $\tau_* > 0.045$, the gravel is considered to be mobile.

4.3. Mobility Potential of Sand as Bed Load and in Suspension

We can also examine the potential mobility of sand as bed load in the reach using equation (10). The median size of sand in the reach is 0.383 mm [*Venditti and Church*, 2014]. Sand can be carried as bed load when $\tau_*/\tau_{*c} > 1$. According to *Church* [2006], channels are bed load dominated (BLD) when $1 < \tau_*/\tau_{*c} < 3$, mixed load dominated (MXD) when $3 < \tau_*/\tau_{*c} < 33$, and suspension dominated (SSD) when $\tau_*/\tau_{*c} > 33$. Figure 9 shows that at low flow (FC1), the channel is clearly bed load dominated for sand, with some locations where a MXD condition can occur. At higher flows, FC2, FC3, and FC4, the channel shifts into the upper range for a MXD channel. During low flow following the freshet (FC5), the channel shifts into the lower range of a MXD system. The results suggest that sand is being moved as bed load throughout the reach, even at the low flows.

We can examine the potential for sand in suspension by comparing the shear velocity against the settling velocity of the sand w_s. Sand can be suspended when $u_{*s}/w_s > 1$ [*Bagnold*, 1966; *Nino and Garcia*, 1998; *Lopez and Garcia*, 2001]. It is difficult to assess what values of u_{*s}/w_s correspond with the BLD, MXD, and SSD classifications of *Church* [2006], which were intended as classifications of the dominant modes of sediment flux at the reach scale and not as grain size specific suspension criteria. Therefore, in order to assess the mobility of sand in suspension, we use $u_{*s}/w_s > 1$ as a suspension criterion, but we base the threshold for significant suspension on a simple advection length scale for suspended sediment calculated as

$$A = \frac{h}{w_s}\overline{u}. \tag{13}$$

where w_s was calculated from *Dietrich* [1982]. The primary advantage of using this simple advection length scale is that it incorporates the dimensions of the channel, velocity, and a measure of the grain size. Sediment sizes with A~O(10) m (meaning order 10 meters), much less than the channel width scale, have $1 < u_{*s}/w_s < 2$, which we interpret as a "lower" mixed load condition with bed load and some minor suspension. Sediment sizes with longer advection lengths scales, O(100) m, approximately the channel width scale, have $2 < u_{*s}/w_s < 5$, and we interpret this as a moderate suspended or "upper" mixed load condition because the suspended

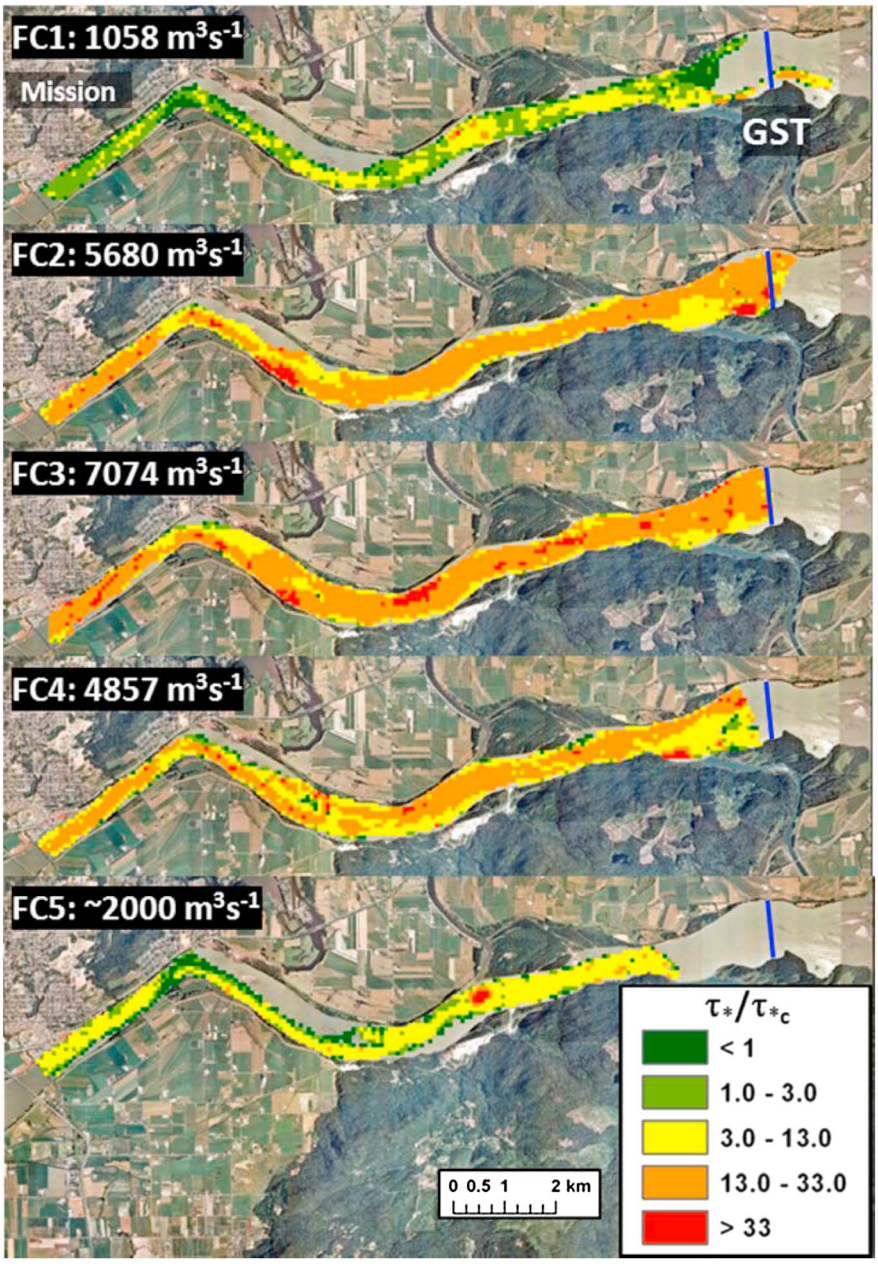

Figure 9. Transport stage τ_*/τ_{*c} of the median sand size in the reach (0.383 mm).

sediment transport length scales are so long. Sediment sizes with A~O(1000) m or longer, much larger than the channel width scale, have $u_{*s}/w_s > 5$. We consider this a substantial suspension condition for the grain size because these sediment sizes can be transported several kilometers before being deposited on the bed. These sizes are likely carried as washload in the channel. These definitions of lower mixed load, upper mixed, or moderate suspension and substantial suspension are analogous to the reach scale classifications of *Church* [2006] for lower MXD, upper MXD, and SSD channels. While the specific ranges of u_{*s}/w_s and A we provide are specific to the Fraser, the conceptual framework that underlies the interpretation of the values in relation to the channel dimensions, velocity, and a measure of the grain size can be applied to any river system.

Figure 10 shows u_{*s}/w_s for the median sand size in the reach (0.383 mm). At low flow (FC1), there is no potential for suspension of this size class according to our criteria. As flows increase (FC2, FC3, and FC4), the reach has the potential for a lower mixed load condition, with some patches with an upper mixed load condition for the median sand size. This suggests that the median sediment size can be carried as both

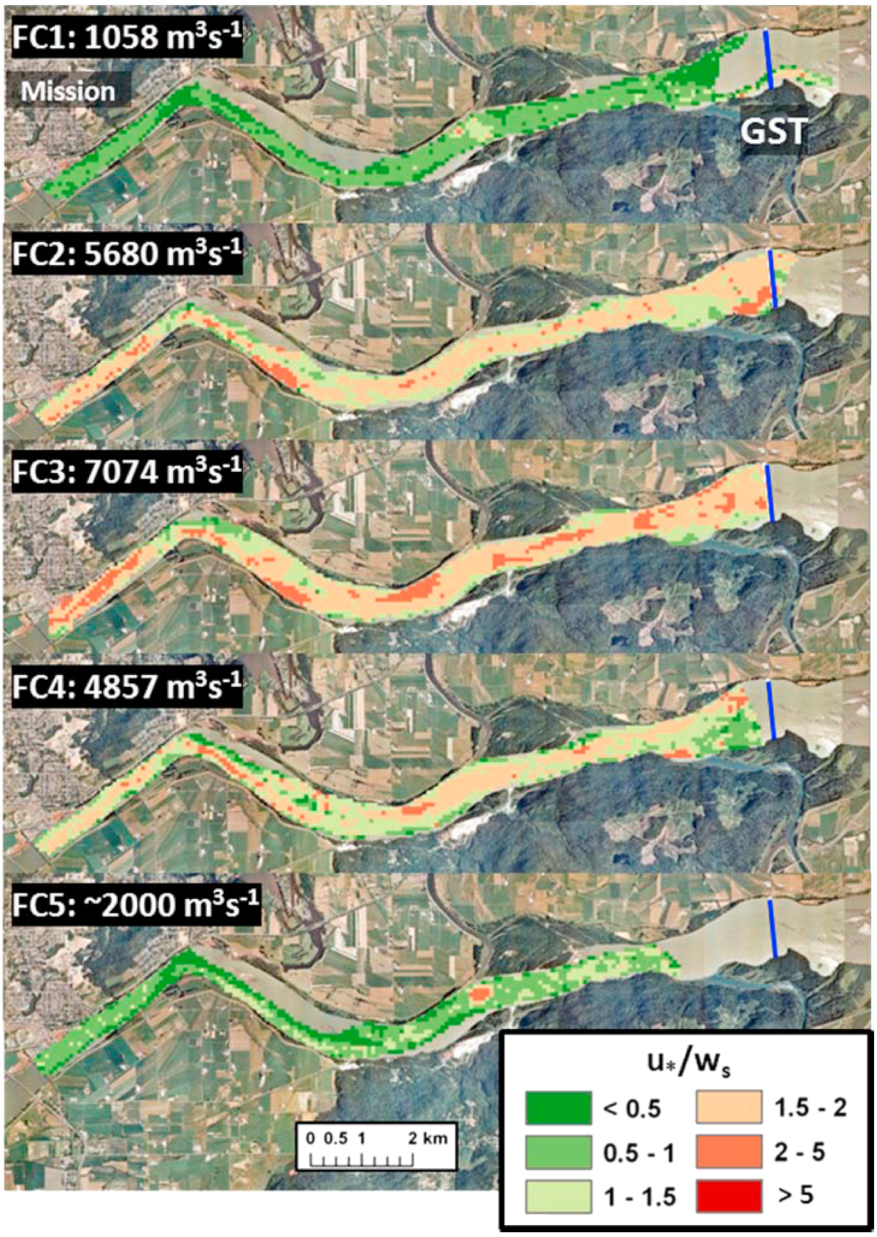

Figure 10. Suspension potential of the median sand size (0.383 mm) in the river.

bed load and suspended load throughout most of the freshet. At no time does the flow have the potential to carry the median bed material size distances approaching the channel width. At low flow, on the receding limb of the freshet hydrograph, there is a weak downstream gradient in u_{*s}/w_s, where it goes from a lower mixed load condition to one where there is no suspension potential of the median sand size. There are no other obvious downstream gradients.

We explored the potential mobility of sand in the reach for various grain sizes between 0.063 and 2 mm at low flow (FC1) and high flow (FC3) (Figure 11) and plotted the advection length scale for each size class shown (Figure 12). At low flow, sediment $\geq D_{50}$ for sand (0.383 mm) cannot be suspended in the reach (see maps for 0.5, 1, and 2 mm). Sand finer than the median (0.125 to 0.250 mm) can be suspended but it is a lower mixed load condition (A is 418 and 140 m, respectively). There is the potential for substantial suspension of 0.063 mm sand, which has $A \approx 1.5$ km. At high flow, sediment $\geq D_{50}$ for sand can be suspended in the reach, but sediment >0.500 mm cannot. For sediment sizes $<D_{50}$, $u_{*s}/w_s > 2.0$ for the

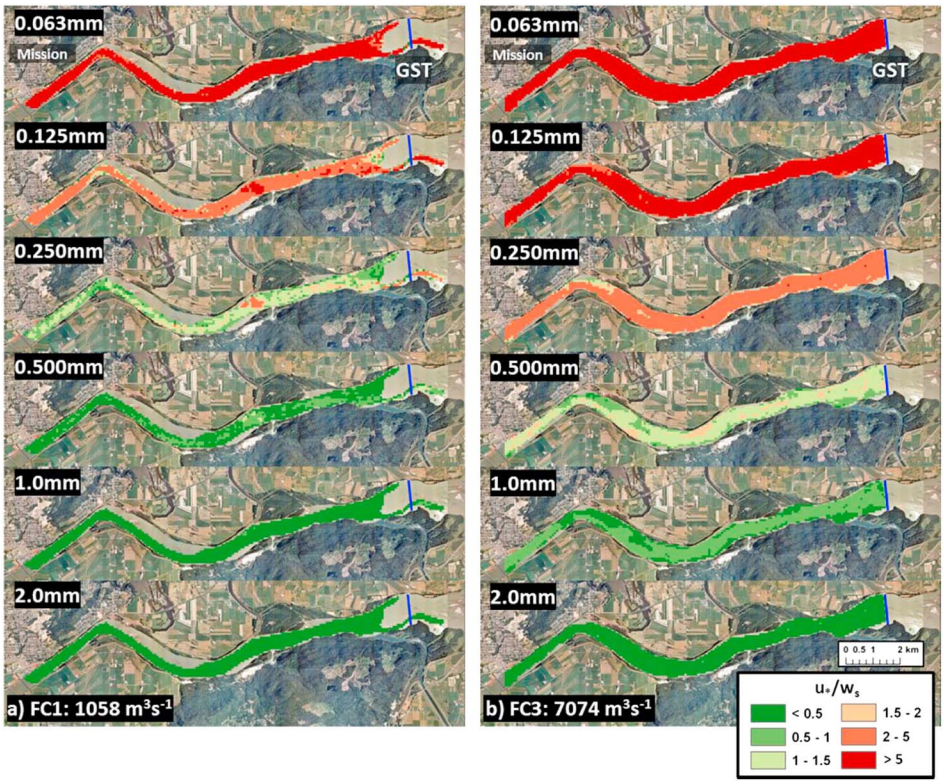

Figure 11. Suspension potential of various grain sizes in the reach.

whole reach at high flow, indicating a moderate potential for suspension and an upper mixed load condition. Advection length scales for 0.250 mm sand are less than the channel width. However, advection length scales for 0.063 and 0.125 mm sand are 4.7 and 1.4 km, suggesting the potential for substantial suspension. *McLean et al.* [1999] showed that the bed material/washload division at Mission (RK 85) was ~0.180 mm based on the near absence of finer size classes in the bed material (<10%). Our observations confirm this, indicating that our classification based on advection length scales is robust.

4.4. Measured Suspended Sediment Flux

The patterns we observe in the potential for sand mobility in suspension should be resolved in our observation of suspended sediment flux using the calibrated ADCP. Figure 13 shows ADCP-measured suspended sediment flux per unit width of channel, q_s. As with velocity and shear stress, q_s increases from FC1 to FC2 to FC3. Unit sediment flux then declines from FC3 to FC4 to FC5. High values of q_s occur along the sinuous thalweg and are highest through Hatzic Bend and the Mission Reach, where the channel is the narrowest. Figure 14a shows the total sediment flux in the channel Q_s (q_s summed across the channel) for all five field campaigns. There is a clear downstream decline in Q_s during FC1 and FC5 that is statistically significant at the 95% confidence interval. Substantial variability in Q_s during FC2, FC3, and FC4 masks any downstream decline

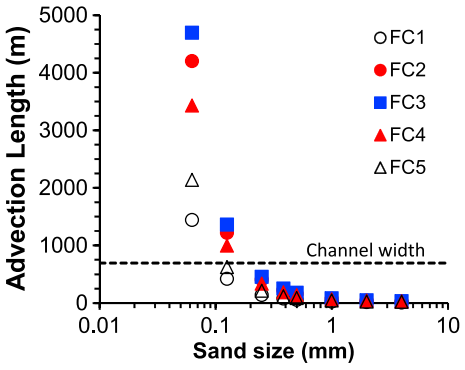

Figure 12. Reach-averaged advection length scale for a variety of different sand grain sizes calculated using equation (13) and the mean velocity and flow depth in the diffuse extension.

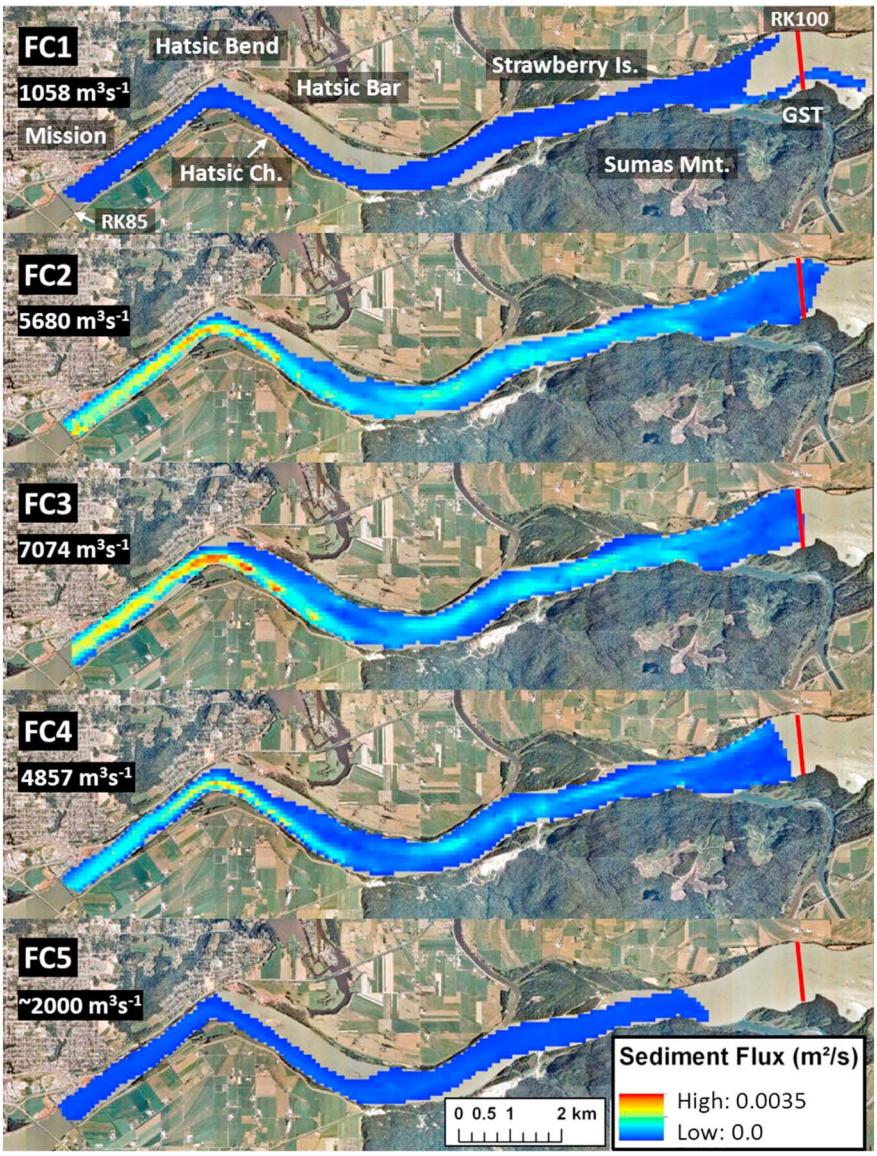

Figure 13. Suspended sediment flux per unit width of the river for all field campaigns interpolated at 80 m resolution.

during the high flow campaigns, and trends are not statistically significant. Similarly, there is a weak statistically significant downstream gradient in the shear stress of 0.1 Pa/km at low flow but no obvious downstream gradient at high flow (Figure 14b).

The anticipated downstream gradient in suspended sand flux, delivering sand to the bed, appears not to occur in this reach of the Fraser River. The reason for this is the short advection length scales for bed material in the diffuse extension reach. It is clear that fine sand moves through the reach year-round, while the coarser sand sizes escape the bed only sporadically and at high flow in this reach.

5. Discussion

5.1. How Does Gravel Mobility Influence the Morphology of Abrupt Gravel-Sand Transitions?

Downstream of the abrupt gravel-sand transition in the Fraser River, the median size of subsurface bed material from the gravel-bedded reach is immobile, suggesting that gravel is generally immobile there. We are interested in the mobility of the subsurface bed material because it is closer to the bed load size distribution than is the generally coarser bed surface size distribution [*Parker et al.*, 1982; *Parker*, 2008].

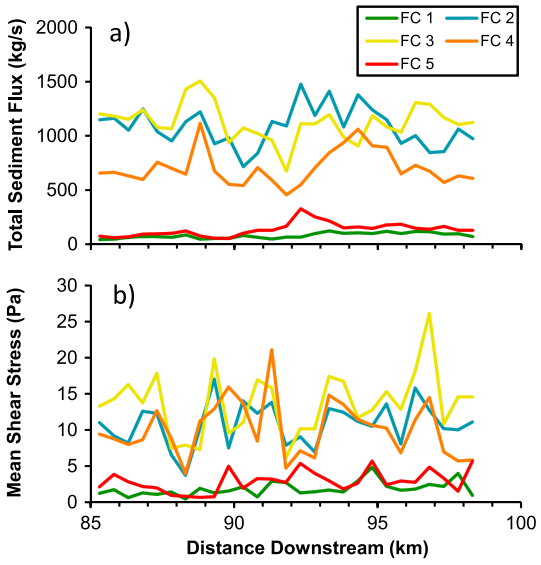

Figure 14. (a) Suspended sediment flux summed across the channel and (b) the mean cross-sectional shear stress.

Venditti and Church [2014] noted that the mean median subsurface bed material size (D_{50sub}) of samples collected by *McLean* [1990] in the gravel-bedded reach is 16.1 mm. Bed material samples from Yaalstick Bar have $D_{50sub} = 12$ mm, while the surface median size is 20 mm [*Church and Ham*, 2004]. However, the downstream fining trend of the subsurface material shown in *Venditti and Church* [2014] suggests that D_{50sub} on Yaalstick Bar is closer to 10 mm. If we accept that the potential mobility of the median particle size defines the mobility of a gravel mixture and we ignore the effect sand may have on the mobility of gravel, Figure 15 suggests that a 10 mm gravel mixture could be marginally mobile at a few locations in the downstream reach. Larger sizes (12 mm and 16 mm) would not be mobile. If the presence of sand reduces the critical Shields stress required for entrainment to 0.03, larger areas of the bed could be mobile, but there is not a reach length connected thread that would be mobile.

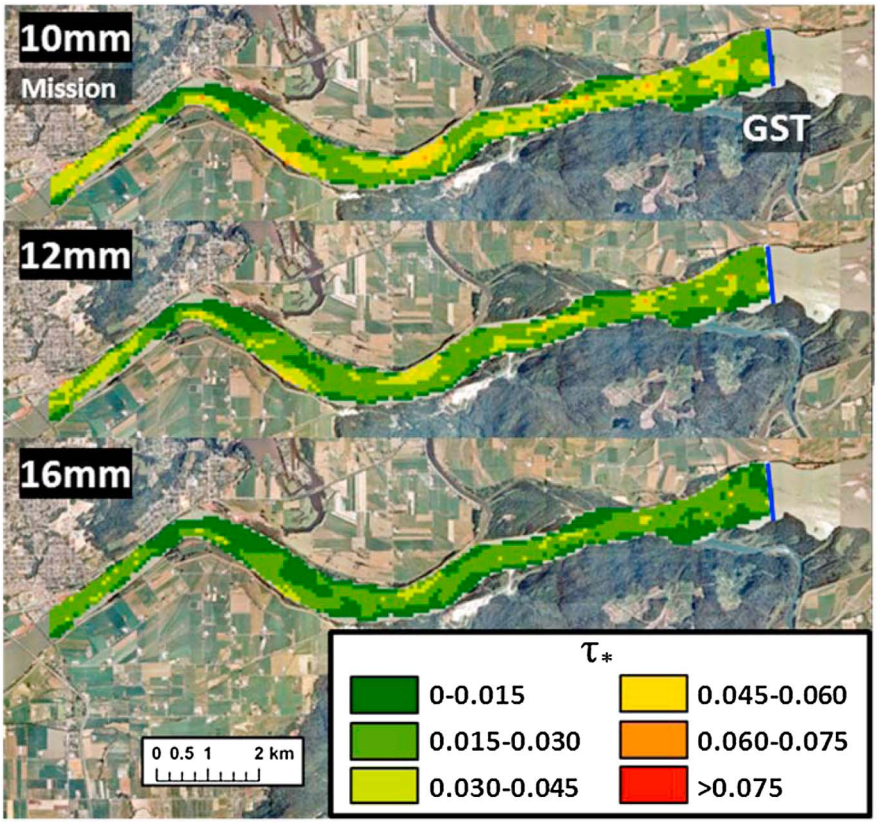

Figure 15. Shields stress for various individual subsurface gravel sizes at high flow (FC3: 7074 $m^3 s^{-1}$) in the study reach. Where $\tau_* > 0.045$, the gravel mixture in the reach is potentially mobile.

The fact that the median bed material size is immobile in the reach indicates that the gravel mixture is not mobile beyond RK 100.5 (the termination of Yaalstrick Bar). This sets the position of the primary transition from a gravel to a sand bed. Why is the gravel not mobile beyond this point? It is likely that the river simply runs out of gravel to deposit because as the river approaches base level, the shear stress is too low to sustain onward transport. The deposition of gravel then induces a further decline in shear stress which leads to the sharp discontinuity in slope documented by *Venditti and Church* [2014] at the upstream end of the diffuse transition reach. The grain size gap in the gravel-bedded reach [*McLean et al.*, 1999], which is common in gravel-bedded rivers [*Shaw and Kellerhals*, 1982; *Wolcott*, 1988], reinforces the sharpness of the transition because gravel finer than ~10 mm is not abundant in the supply to the study reach.

Venditti and Church [2014] suggested that the occurrence of gravel patches downstream of the primary shift from a framework supported gravel to a sand deposit is due to the "superior mobility" of gravel over sand [*Ikeda*, 1984]. It is well known that sand, in sufficient quantities, reduces the threshold for motion of gravel [*Jackson and Beschta*, 1984; *Ikeda*, 1984; *Iseya and Ikeda*, 1987; *Wilcock*, 1998; *Wilcock and McArdell*, 1993; *Wilcock and McArdell*, 1997; *Wilcock et al.*, 2001; *Wilcock and Kenworthy*, 2002; *Wilcock and Crowe*, 2003; *Curran and Wilcock*, 2005]. Confirming earlier speculation, *Venditti et al.* [2010] demonstrated that the mechanism for this is smoothing of the bed by finer particles, increasing flow velocities and drag on larger particles, leading to their entrainment and transport. Our shear stress calculations support the speculation of *Venditti and Church* [2014] that gravel is leaking out of the gravel wedge and riding over the sand because the shear stresses are not sufficient to move the gravel mixture beyond the wedge (Figure 10). At high flow, stresses are locally sufficient to move fine gravel—that is, material up to 8 mm in size (Figure 8b). However, patches of gravel do not generally coincide with patches of locally high shear stresses (Figure 6), so it must be formed by gravel riding over sand. The patterns of local gravel deposits in the study reach—including grains considerably larger than 10 mm—in pools and on downstream bar heads [*Venditti and Church*, 2014] must be influenced by processes other than the spatial variability in shear stress; the obvious mechanism is the movement of gravel over sand, with reduced values of τ_{*_c} for such individual grains.

5.2. What Is the Pattern of Sand Deposition to the Bed?

The median sand size (0.383 mm) can be carried as bed load in the river downstream of the abrupt gravel-sand transition at all but the lowest flows (Figure 9). At high flows, the median-sized sand can also be transported in suspension (Figure 10), but not for distances exceeding the channel width (Figure 12), which confirms its status as bed material. Examination of grain size specific potential mobility of sand suggests that at high flow, sediment coarser than median sand is being deposited on the bed, thereby creating the sand bed downstream of the gravel wedge.

However, the absence of downstream gradients in shear stress and sediment flux in the diffuse extension is surprising and suggests that the bed is not formed by gradual deposition of sand but rather en masse deposition at the end of the gravel wedge. The advection length scale calculations support this idea. Figure 12 shows that the relation between advection length scale and grain size is highly nonlinear, with washload and bed material sizes forming distinct asymptotes. The transport lengths of most sand sizes are less than the channel width in the diffuse extension, with the exception of the finest grain sizes, which are not resident in the bed. The suspension advection lengths for the coarser sands indicate that they abruptly go to the bed when they advect off the end of the gravel wedge in the vicinity of RK 100.5, while the sand remaining in suspension continues as washload. The difference in advection length scales we calculate for the various grain sizes (Figure 12) should lead to a downstream fining sequence through the study reach. However, this fining would occur over less than a channel width, immediately downstream of the primary transition. Identifying this pattern is beyond the resolution of our measurements, but it would logically enhance the abruptness of the primary gravel-sand transition.

Further support for the foregoing analysis is gained from the interannual variation in sand transport through the system. Figure 16 plots the change in bed elevation between 2003 and 2008 (years for which we have data available in the study reach collected by Public Works, Canada). The 2003 freshet was low with a return period of 1.7 years, and the 2007 and 2008 freshets were high freshets with return periods of 12.5 and 8.3 years, respectively. The broad pattern of bed elevation change shows that sand had accumulated in the upstream end of the transition reach in 2003—lending credence to our conclusion above that sand

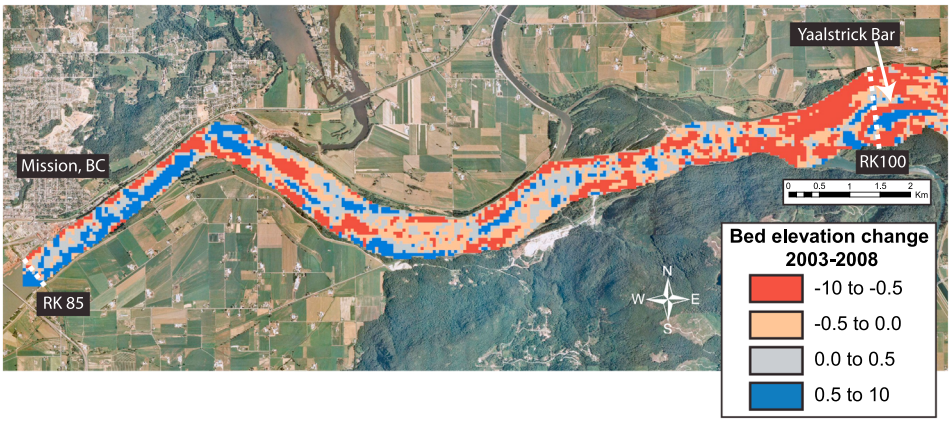

Figure 16. Changes in bed elevation between 2003 and 2008 in meters. The data were derived from transects that were surveyed by Public Works Canada, interpolated using the raw transect data, and bed contours lines aligned with the channel to remove "ringing" in the interpolated surface. The scale is selected to conservatively separate significant bed elevation changes in the reach (dark red and blue) and changes that are likely within the range of error associated with the survey and subsequent interpolation (light blue and red).

quickly goes to the bed around RK100.5. In the high 2008 freshet, that sand was evacuated from the upper end of the study reach and deposited toward its lower end. Similar large fluctuations in bed level—up to 2 m—in the 2 km reach immediately downstream from RK100.5, have been documented in earlier work [*McLean*, 1990; *Ham*, 2005]. These observations suggest that sand is staged through the diffuse transition reach, accumulating at the termination of the gravel reach in low to moderate freshets and moving downstream during the high freshets. This highlights the linkage between sediment supply and flow variability and the role it plays in channel morphology.

5.3. Can Abrupt Gravel-Sand Transitions Emerge due to Changes in Sediment Suspension?

It has been widely argued that in bed load-dominated systems, abrupt gravel-sand transitions emerge due to sorting of a bimodal sediment by size-selective bed load transport [*Sambrook Smith and Ferguson*, 1995; *Ferguson et al.*, 1996, 1998; *Wilcock*, 1998; *Ferguson*, 2003; *Ferguson et al.*, 2011] such that the river "runs out of gravel" [*Paola et al.*, 1992; *Cui and Parker*, 1998]. Our results do not contradict this general idea. It is probable that the sedimentology of gravel-sand transitions depends closely on the necessity for a gravel-bedded river to adopt a steeper slope than a sand-bedded river of equivalent size in order to pass the incoming bed material load. The change in gradient at the limit of gravel advance also sets the condition for sand deposition on the bed. We consider that sand deposition to the bed plays an important role in the emergence of gravel-sand transitions. Gravel-bedded—and gravel transporting—reaches necessarily assume a gradient that generates shear stresses capable of keeping sand sized particles in suspension, thus discouraging sand deposition in the thalweg. Sand, suspended in the gravel reach, cannot be maintained in suspension beyond the limit of the steep gradient created by the gravel-bedded reach of the river and is delivered en masse to the bed. As such, the respective gravel-bedded and sand-bedded slopes are those required to convey the incoming bed material load. The channel slope required to convey the gravel load dictates the location of the gravel wedge, which in turn determines the location of the main shift from framework supported gravel to a sand bed.

6. Conclusions

We have presented spatially resolved measurements of velocity, shear stress, sediment mobility, and suspended sediment flux immediately downstream of an abrupt transition from a framework-supported gravel bed to a sand bed supporting a secondary gravel mode. The sand-bedded portion of the river has patches of gravel that constitute the sediment bimodality often observed as a part of gravel-sand transitions and defines a diffuse extension of the primary transition. Our observations lead to the following conclusions:

1. General movement of the gravel mixture cannot continue downstream of the primary grain size transition because the shear stress is too low to maintain movement of the median-sized gravel.

2. Gravel clasts evidently do move in the diffuse extension where gravel patches are formed. Because the shear stress is too low to move the gravel mixture, we attribute the presence of gravel to the effect of sand on gravel clast mobility.
3. There are no downstream gradients in shear stress or suspended sediment flux in the study reach that would suggest that sand is raining out of suspension throughout the diffuse extension.
4. Advection length scales for the sand bed material are O(10 to 100) m, suggesting that this sand should deposit at the upstream end of the diffuse extension reach.
5. Our examination of interannual bed elevation change in the diffuse extension suggests that sand is staged through the reach, deposited en masse at the upstream end of the reach during low freshets, and evacuated during high freshets.
6. Our coupling of a suspension criterion and an advection length scale successfully links the division between bed material and wash load to channel geometry, grain size, and velocity. Our method could be used as an objective way to divide these components of the load.

The prevailing theory for why abrupt gravel-sand transitions emerge is based on bed load sorting of a bimodal sediment. We argue that sediment deposition from suspension can play a more important role in the emergence of abrupt gravel-sand transitions than has previously been acknowledged.

Acknowledgments

This work was supported by the National Sciences and Engineering Research Council of Canada discovery grant to J.G.V. The field campaign was undertaken by N.D., J.G.V., and M.C. with field assistance from Martin Lin, Sally Haggarstone, Megan Hendershot, Robert Humphries. and Ray Kostaschuk (all from SFU). Data were initially processed by N.D. with assistance from C.D.R., and subsequent analysis was undertaken by J.G.V. with assistance from Malcolm Little (SFU). The paper was written by J.G.V. with input from the coauthors. We thank our field and research assistants for their contributions. All data presented in this paper are freely available from the corresponding author (J.V.). The authors thank the Associate Editor and reviewers for insightful comments that sharpened our interpretation of the data.

References

Attard, M. A., J. G. Venditti, and M. Church (2014), Suspended sediment transport in Fraser river at mission, British Columbia: New observations and comparison to historical records, *Can. J. Water Resour.*, doi:10.1080/07011784.2014.942105.

Bagnold, R. A. (1966), *An Approach to the Sediment Transport Problem for General Physics*, *U.S. Geol. Surv. Prof. Pap., 422-I*, Geological Survey, Washington, D. C.

Bradley, R. W., J. G. Venditti, R. A. Kostaschuk, M. Church, M. Hendershot, and M. A. Allison (2013), Flow and sediment suspension events over low-angle dunes: Fraser Estuary, Canada, *J. Geophys. Res. Earth Surf.*, *118*, 1693–1709, doi:10.1002/jgrf.20118.

Brierley, G. J., and E. J. Hickin (1985), Downstream gradation of particle sizes in the Squamish River, British Columbia, *Earth Surf. Processes Landforms*, *10*, 597–606.

Church, M. (2006), Bed material transport and the morphology of alluvial river channels, *Annu. Rev. Earth Planet. Sci.*, *34*, 325–354, doi:10.1146/annurev.earth.33.092203.122721.

Church, M., and D. G. Ham (2004), Atlas of the alluvial gravel-bed reach of Fraser River in the Lower Mainland, Dept. Geography, The University of British Columbia. Fraser River Project Report: ii+55 pp. [Available at www.geog.ubc.ca/fraserriver/reports.]

Church, M., and R. Kellerhals (1978), On the statistics of grain size variation along a gravel river, *Can. J. Earth Sci.*, *15*, 1151–1160.

Church, M., M. A. Hassan, and J. F. Wolcott (1998), Stabilizing self-organized structures in gravel-bed stream channels, *Water Resour. Res.*, *34*, 3169–3179.

Cui, Y., and G. Parker (1998), The arrested gravel front: Stable gravel-sand transitions in rivers Part II: General numerical solution, *J. Hydraul. Res.*, *36*, 159–182.

Curran, J. C., and P. R. Wilcock (2005), The effect of sand supply on transport rates in a gravel-bed channel, *J. Hydraul. Eng.*, *131*, 961–967, doi:10.1061/(ASCE)07339429(2005)131:11(961).

Dade, W. B., and P. F. Friend (1998), Grain size, sediment transport regime and channel slope in alluvial rivers, *J. Geol.*, *106*, 661–675.

Dietrich, W. E. (1982), Settling velocity of natural particles, *Water Resour. Res.*, *18*, 1615–1626, doi:10.1029/WR018i006p01615.

Dietrich, W. E., and P. Whiting (1989), Boundary shear stress and sediment transport in river meanders of sand and gravel, in *River Meandering*, *Water Resour. Monogr.*, vol. 12, edited by S. Ikeda and G. Parker, pp. 1–50, AGU, Washington, D. C.

Domarad, N. (2011), Flow and suspended sediment transport through the gravel-sand transition in the Fraser River, British Columbia, MSc thesis, Simon Fraser Univ.

Ferguson, R., T. Hoey, S. Wathen, and A. Werrity (1996), Field evidence for rapid downstream fining of river gravels through selective transport, *Geology*, *24*, 179–182.

Ferguson, R. I. (2003), Emergence of abrupt gravel to sand transitions along rivers through sorting process, *Geology*, *31*, 159–162.

Ferguson, R. I., T. B. Hoey, S. J. Wathen, A. Werritty, R. I. Hardwick, and G. H. Sambrook Smith (1998), Downstream fining of river gravels: An integrated field lab and modeling study, in *Gravel Bed Rivers in the Environment: Proceedings of the 4th International Workshop on Gravel-bed Rivers*, edited by P. Klingeman et al., pp. 85–114, Water Resour. Publ., Lakewood, Colo.

Ferguson, R. I., D. J. Bloomer, and M. Church (2011), Evolution of an advancing gravel front: Observations from Vedder Canal, British Columbia, *Earth Surf. Processes Landforms*, *36*, 1172–1182.

Flammer, G. H. (1962), *Ultrasonic Measurement of Suspended Sediment*, *U.S. Geol. Surv. Bull. 1141-A*, 48 pp., Washington, D. C.

Frings, R. M. (2011), Sedimentary characteristics of the gravel-sand transition in the river Rhine, *J. Sediment. Res.*, *81*, 52–63, doi:10.2110/jsr.2011.2.

Gartner, J. W. (2004), Estimating suspended solids concentrations from backscatter intensity measured by acoustic Doppler current profiler in San Francisco Bay, California, *Mar. Geol.*, *211*, 169–187, doi:10.1016/j.margeo.2004.07.001.

Gran, K. B. (2012), Strong seasonality in sand loading and resulting feedback on sediment transport, bed texture, and channel planform at Mount Pinatubo Philippines, *Earth Surf. Processes Landforms*, *37*, 1012–1022, doi:10.1002/esp.3241.

Gran, K. B., D. R. Montgomery, and D. G. Sutherland (2006), Channel bed evolution and sediment transport under declining sand inputs, *Water Resour. Res.*, *42*, W10407, doi:10.1029/2005WR004306.

Ham, D. G. (2005), Morphodynamics and sediment transport in a wandering gravel-bed channel: Fraser River, B.C. PhD thesis, 210 pp., The Univ. of British Columbia, Vancouver, B. C.

Howard, A. M. (1980), Thresholds in river regimes, in *Thresholds in Geomorphology*, edited by D. Coates and J. Vitek, pp. 227–258, Allen and Unwin, Boston.

Ikeda, H. (1984), *Flume Experiments on the Superior Mobility of Sediment Mixtures*, *Ann. Rep. Inst. Geosci.*, vol. 10, pp. 53–56, Univ. of Tsukuba, Tsukuba, Japan.

Iseya, F., and H. Ikeda (1987), Pulsations in bed load transport rates induced by a longitudinal sediment sorting: A flume study using sand and gravel mixtures, *Geogr. Ann., Ser. A, Phys. Geogr.*, *69*, 15–27, doi:10.2307/521363.
Jackson, W. L., and R. L. Beschta (1984), Influences of increased sand delivery on the morphology of sand and gravel channels, *J. Am. Water Resour. Assoc.*, *20*, 527–533, doi:10.1111/j.1752-1688.1984.tb02835.x.
Jerolmack, D. J., and T. A. Brzinski (2010), Equivalence of abrupt grain size transitions in alluvial rivers and eolian sand seas: A hypothesis, *Geology*, *38*, 719–722.
Kashyap, S., G. Constantinescu, C. D. Rennie, G. Post, and R. Townsend (2012), Influence of channel aspect ratio and curvature on flow, secondary circulation and bed shear stress in a bend, *J. Hydraul. Eng.*, *138*, 1045–1059.
Knighton, D. A. (1998), The gravel-sand transition in a disturbed catchment, *Geomorphology*, *27*, 325–341.
Kodama, Y. (1994), Downstream changes in the lithology and grain size of fluvial gravels, the Waterase River, Japan: Evidence of the role of abrasion in downstream fining, *J. Sediment. Res.*, *A64*, 68–75.
Lopez, F., and M. Garcia (2001), Risk of sediment erosion and suspension in turbulent flows, *J. Hydraul. Eng.*, *127*, 231–235.
McLean, D. G. (1990), Channel instability on lower Fraser River, PhD thesis, 290 pp., The Univ. of British Columbia, Vancouver, B. C.
McLean, D. G., and M. Church (1999), Sediment transport along lower Fraser River 2. Estimates based on the long-term gravel budget, *Water Resour Res.*, *35*, doi:10.1029/1999WR900102.
McLean, D. G., M. Church, and B. Tassone (1999), Sediment transport along lower Fraser River. 1. Measurements and hydraulic computations, *Water Resour. Res.*, *35*, 2533–2548, doi:10.1029/1999WR900101.
Miller, M. C., I. N. McCave, and P. D. Komar (1977), Threshold of sediment motion under unindirectional currents, *Sedimentology*, *41*, 883–903.
Nino, Y., and M. H. Garcia (1998), On England's analysis of turbulent energy and suspended load, *J. Hydraul. Eng.*, *124*, 480–483.
Northwest Hydraulic Consultants (2008), Comprehensive review of Fraser River at Hope, flood hydrology and flows – scoping study, Report prepared for British Columbia Ministry of Environment, 25 pp + tables, figures.
Paola, C., G. Parker, R. Seal, S. K. Sinha, J. B. Southard, and P. R. Wilcock (1992), Downstream fining by selective deposition in a laboratory flume, *Science*, *258*, 1757–1760.
Parker, G. (2008), Transport of gravel and sediment mixtures, in *Sedimentation Engineering: Theories, Measurements, Modeling and Practice*, *ASCE Manual Rep. Eng. Practice*, vol. 110, edited by M. H. Garcia, chap. 3, pp. 165–264, Am. Soc. of Civ. Eng, Reston, Va.
Parker, G., P. C. Klingman, and D. G. McLean (1982), Bedload and size distribution in paved gravel-bed streams: American Society of Civil Engineers, *J. Hydraul. Div.*, *108*(HY4), 544–571.
Rennie, C. D., and M. Church (2010), Mapping spatial distributions and uncertainty of water and sediment flux in a large gravel-bed river reach using an aDcp, *J. Geophys. Res.*, *115*, F03035, doi:10.1029/2009JF001556.
Rennie, C. D., and R. G. Millar (2004), Measurement of the spatial distribution of fluvial bed load transport velocity in both sand and gravel, *Earth Surf. Processes Landforms*, *29*, 1173–1193.
Rice, S., and M. Church (1998), Grain size along two gravel-bed rivers: Statistical variation, spatial pattern and sedimentary links, *Earth Surf. Processes Landforms*, *23*, 345–365.
Sambrook Smith, G. H., and R. I. Ferguson (1995), The gravel-sand transition along river channels, *J. Sediment. Res.*, *A65*, 423–430.
Sambrook Smith, G. H., and R. I. Ferguson (1996), The gravel-sand transition: flume study of channel response to reduced slope, *Geomorphology*, *16*, 147–159.
Schulkin, M., and H. W. Marsh (1962), Sound absorption in seawater, *J. Acoust. Soc. Am.*, *34*, 864–865.
Shaw, J., and R. Kellerhals (1982), The composition of recent alluvial gravels in Alberta River beds, *Alberta Res. Counc. Bull.*, *41*, 151.
Sibson, R. (1981), Chapter 2: A brief description of natural neighbor interpolation, in *Interpolating Multivariate Data*, edited by V. Barnett, pp. 21–36, John Wiley, Chichester, U. K.
Sime, L. C., R. I. Ferguson, and M. Church (2007), Estimating shear stress from moving-boat acoustic Doppler velocity measurements in a large gravel-bed river, *Water Resour. Res.*, *43*, W03418, doi:10.1029/2006WR005069.
Sternberg, H. (1875), Untersuchungen Uber Langen-und Querprofil geschiebefuhrender Flusse, Zeitschrift fur Bauwesen XXV, 483–506.
Thorne, P. D., and D. M. Hanes (2002), A review of acoustic measurements of small-scale sediment processes, *Cont. Shelf Res.*, *22*, 603–632.
Urick, R. J. (1948), The absorption of sound in suspensions of irregular particles, *J. Acoust. Soc. Am.*, *20*, 283–289.
van Rijn, L. C. (1993), *Principles of Sediment Transport in Rivers*, Estuaries and Coastal Seas, Aqua, Amsterdam.
Venditti, J. G., and M. Church (2014), Morphology and controls on the position of a gravel-sand transition: Fraser River, British Columbia, *J. Geophys. Res. Earth Surf.*, *119*, 1959–1976, doi:10.1002/2014JF003147.
Venditti, J. G., W. E. Dietrich, P. A. Nelson, M. A. Wydzga, J. Fadde, and L. Sklar (2010), Mobilization of coarse surface layers in gravel-bedded rivers by finer gravel bed load, *Water Resour. Res.*, *46*, W07506, doi:10.1029/2009WR008329.
Wall, G. R., E. A. Nystrom, and S. Litten (2006), Use of an ADCP to compute suspended sediment discharge in the tidal Hudson River, New York, U.S. Geol. Surv. Scientific Invest. Rep. 2006–5055, 16 pp.
Watson, D. (1992), *Contouring: A Guide to the Analysis and Display of Spatial Data*, Pergamon Press, London.
Wilcock, P. R. (1998), Two-fraction model of initial sediment motion in gravel-bed rivers, *Science*, *280*, 410–412.
Wilcock, P. R., and J. C. Crowe (2003), A surface-based transport model for sand and gravel, *J. Hydraul. Eng.*, *129*, 120–128, doi:10.1061/(ASCE)0733-9429(2003)129:2(120).
Wilcock, P. R., and S. T. Kenworthy (2002), A two-fraction model for the transport of sand/gravel mixtures, *Water Resour. Res.*, *38*, 1194, doi:10.1029/2001WR000684.
Wilcock, P. R., and B. W. McArdell (1993), Surface-based fractional transport rates: Mobilization threshold and partial transport of a sand-gravel sediment, *Water Resour. Res.*, *29*, 1297–1312, doi:10.1029/92WR02748.
Wilcock, P. R., and B. W. McArdell (1997), Partial transport of a sand/gravel sediment, *Water Resour. Res.*, *33*, 235–245, doi:10.1029/96WR02672.
Wilcock, P. R., S. T. Kenworthy, and J. C. Crowe (2001), Experimental study of the transport of mixed sand and gravel, *Water Resour. Res.*, *37*, 3349–3358, doi:10.1029/2001WR000683.
Wolcott, J. (1988), Non-fluvial control of bimodal grain size distributions in river bed gravels, *J. Sediment. Petrol.*, *58*, 979–984.
Yalin, M. S., and E. Karahan (1979), Inception of sediment transport, *J. Hydraul. Div., Am. Soc. Civil Eng.*, *105*, 1433–1443.
Yatsu, E. (1955), On the longitudinal profile of the graded river, *Am. Geophys. Union Trans.*, *36*, 655–663.
Yatsu, E. (1957), On the discontinuity of grain size frequency distribution of fluvial deposits and its geomorphological significance, Proceedings of the International Geophysical Union Regional Conference, Tokyo, Japan, pp. 224–237.